RESEARCH ARTICLE | JANUARY 06 2026

Two-state reaction path search using a quantum Monte Carlo-inspired approach

Denis S. Tikhonov ; Robin Santra

J. Chem. Phys. 164, 014114 (2026)
https://doi.org/10.1063/5.0293846

The Journal of Chemical Physics ARTICLE pubs.aip.org/aip/jcp

Two-state reaction path search using a quantum Monte Carlo-inspired approach

Cite as: J. Chem. Phys. 164, 014114 (2026); doi: 10.1063/5.0293846
Submitted: 30 July 2025 • Accepted: 13 December 2025 •
Published Online: 6 January 2026

Denis S. Tikhonov[1,2,a)] and Robin Santra[1,2]

AFFILIATIONS

[1] Center for Free-Electron Laser Science CFEL, Deutsches Elektronen-Synchrotron DESY, 22603 Hamburg, Germany
[2] Department of Physics, University of Hamburg, 22607 Hamburg, Germany

[a)] **Author to whom correspondence should be addressed:** denis.tikhonov@desy.de

ABSTRACT

We present an algorithm for finding chemical reaction pathways using a Monte Carlo transition state search (MCTSS) scheme. Our strategy is a bidirectional two-state approach that simultaneously drives two Monte Carlo trajectories from reactants to products, and *vice versa*, until the trajectories meet. The trajectories are driven in a Metropolis-like procedure with transition probabilities based on the real-space diffusion Monte Carlo algorithm. A computationally inexpensive structure preselection procedure is used to guide the two trajectories toward each other. We performed a proof-of-principle demonstration of the MCTSS algorithm for the model two-dimensional double-well potential and for the halogen anion S_N2-substitution in halogenated methane. The MCTSS approach presented here is expected to be particularly useful when employing electronic structure methods that do not provide analytic gradients.

I. INTRODUCTION

Transition state theory (TST), developed almost 100 years ago, is an extremely powerful tool for understanding and describing the kinetics of chemical reactions.[1,2] TST conceptualizes all thermal chemical reactions as proceeding through special points on the potential energy surface (PES), called transition state (TS). Each TS is a stationary point. More specifically, the energy at a TS is maximal along one specific nuclear degree of freedom, called the reaction coordinate, and minimal along all other nuclear coordinates, forming a multidimensional pass between valleys of products and reactants, local minima on the PES. Therefore, searching for these TS's is a central task for computational chemistry, which is important in any branch of chemistry, including homogeneous and heterogeneous catalysis[3–6] and biochemistry.[7]

The TS search is a complicated task, as the conventional minimization/maximization methods cannot be applied for simultaneous maximization along one coordinate and minimization along all the rest of them. Therefore, many special methods have been developed over the years to solve this problem. The first types of methods for TS search are optimization-like routines, such as "Berny optimization" algorithm,[8,9] synchronous transit-guided quasi-Newton search,[10] eigenvector following,[11] and restricted-step partitioned rational function optimization.[12] These quasi-local optimization methods usually require a good initial guess of the TS geometry and a decent estimation of the PES Hessian during the optimization, which makes such search strategies for the TS involve a lot of chemical intuition, ultimately making finding the mechanisms of complicated reactions a work of art.

A handful of methods for finding reaction pathways also rely on molecular dynamics (MD) simulations. Some of those are actually various types of enhanced sampling methods,[13] such as metadynamics[14] and adaptive biasing force,[15] which bias the nuclear motion, such as to push the system toward the desired outcome. One can also use restricted versions of MD, for instance, with milestoning, to probe various reaction pathways.[16,17] Another way to utilize MD is to use high temperatures to provide sampling of the PES landscape and then analyze the trajectories to find various reaction-like events.[18] MD computations are generally quite expensive. Thus, such TS search methods rely on empirical or semi-empirical PES's to reduce the computational cost of the methods.[19] The usage of Monte Carlo (MC) approaches for finding reaction pathways is also not an uncommon way to explore chemical space. These methods, such as the basin hopping MC and its extensions,[20–22] can successfully locate

global minima of multidimensional energy landscapes and even find TS's between local minima.[23]

Another development in reaction path and TS search is the so-called chain-of-states methods, which approximate and optimize a path between reactants and specific products by representing it as a chain-like connected set of structures.[24] The first large set of chain-of-states methods is the nudged elastic band (NEB) method,[25,26] which was later extended to the climbing-image NEB (CI-NEB) or energy-weighted CI-NEB (EW-CI-NEB), doubly NEB (DNEB),[27] etc. approaches.[28,29] The second large set of approaches is from the family of string methods,[30] which later were extended to growing string methods (GSM),[31] and even single-ended GSM (not requiring a reaction product).[32] These developments inspired other two-state methods, which locate the TS by searching structures between the initial and final states of the reaction, such as the binary-image TS search (BITSS) method[33] or geodesic curves construction on the machine-learned PES.[34]

In this work, we present the MC TS search (MCTSS) method, a two-state reaction path search approach based on real-space diffusion MC (DMC),[35] a quantum MC (QMC) algorithm.[36] In particular, the approach developed here is related to the DMC-based smoothing procedure introduced in Ref. 37. In Sec. II, we present the derivation of the approach and the proposed algorithm; in Sec. III, we provide numerical examples by applying an implementation of the approach to the two-dimensional double-well potential and S_N2 substitution in halogenated methane; and in Secs. IV and V, we discuss the results and draw conclusions, respectively.

II. THE APPROACH

To construct our algorithm for the search of reaction pathways between different structures, we will use a framework based on real-space DMC.[35] Let us assume that the nuclear configuration is described by a set of N vectors of nuclear positions $\{\mathbf{r}_n\}_{n=1}^{N}$, where N is the number of nuclei in the system and the nth nucleus has a mass of m_n. We will denote such a configuration by a $3N$-dimensional vector, $\mathbf{R}$. The electronic energy given at configuration $\mathbf{R}$ is given as $V(\mathbf{R})$. The time propagation operator for a time step Δt is given as

$$\hat{U}_{\Delta t} = \exp\left(-\frac{\mathrm{i}\Delta t}{\hbar}\hat{H}\right), \tag{1}$$

where $\hbar = 1.054 \times 10^{-34}$ J/s is the reduced Planck constant, i is the imaginary unit, and $\hat{H} = \hat{T} + \hat{V}$ is the Hamiltonian composed of the kinetic ($\hat{T}$) and potential ($\hat{V}$) energy operators. By taking an imaginary time step, $\Delta t = -\mathrm{i}\tau$, where $\tau = |\Delta t| \geq 0$ is related to the effective inverse temperature $\beta = \tau/\hbar$, we can now compute the unnormalized transition probability from geometry $\mathbf{R}$ to geometry $\mathbf{R}'$ in time Δt as[38]

$$p(\mathbf{R} \to \mathbf{R}') = \left|\langle \mathbf{R}'|\hat{U}_{-\mathrm{i}\tau}|\mathbf{R}\rangle\right|^2 = \left|\langle \mathbf{R}'|\exp\left(-\frac{\tau}{\hbar}\hat{H}\right)|\mathbf{R}\rangle\right|^2. \tag{2}$$

We then take the second-order Trotter decomposition of the exponential operator, namely,[35]

$$\exp\left(-\frac{\tau}{\hbar}\hat{H}\right) \approx \exp\left(-\frac{\tau}{2\hbar}\hat{V}\right)\exp\left(-\frac{\tau}{\hbar}\hat{T}\right)\exp\left(-\frac{\tau}{2\hbar}\hat{V}\right). \tag{3}$$

For position kets $|\mathbf{R}\rangle$, the following expression holds:[38]

$$\exp\left(-\frac{\tau}{2\hbar}\hat{V}\right)|\mathbf{R}\rangle = |\mathbf{R}\rangle\exp\left(-\frac{\tau}{2\hbar}V(\mathbf{R})\right). \tag{4}$$

The kinetic energy evolution integral is given by[38]

$$\begin{aligned}\langle \mathbf{R}'|\exp\left(-\frac{\tau}{\hbar}\hat{T}\right)|\mathbf{R}\rangle &= \underbrace{(\pi\hbar)^{3N/2}\prod_{n=1}^{N} m_n^{3/2}}_{\mathcal{N}} \\ &\quad\times \exp\left(-\sum_{n=1}^{N}\frac{m_n}{2\hbar\tau}(\mathbf{r}_n - \mathbf{r}_n')^2\right) \\ &= \mathcal{N}\exp\left(-\frac{\mathrm{mwMSD}\,(\mathbf{R},\mathbf{R}')}{2\hbar\tau}\right),\end{aligned} \tag{5}$$

where $\mathcal{N}$ is a normalization constant and

$$\mathrm{mwMSD}\,(\mathbf{R},\mathbf{R}') = \sum_{n=1}^{N} m_n(\mathbf{r}_n - \mathbf{r}_n')^2 \tag{6}$$

is the mass-weighted mean square deviation between the two structures $\mathbf{R}$ and $\mathbf{R}'$. As $\mathrm{mwMSD}(\mathbf{R},\mathbf{R}')$ is an orientation-dependent quantity, we take the maximal possible transition probability corresponding to the minimal possible mwMSD value by removing the effects of translation and rotation of the two structures relative to each other. For that, we first center both structures $\mathbf{R}$ and $\mathbf{R}'$ with respect to their centers of mass, and then, we orient one of them with respect to the other using the Kabsh algorithm,[39] which yields a minimal mass-weighted distance (mmwD) of

$$\mathrm{mmwD}\,(\mathbf{R},\mathbf{R}') = \min\left\{\mathrm{mwMSD}\,(\mathbf{R},\mathbf{R}')\right\}. \tag{7}$$

Combining Eqs. (2)–(5) and (7), we arrive at

$$p(\mathbf{R} \to \mathbf{R}') = \mathcal{N}^2\exp\left(-\frac{\tau V(\mathbf{R})}{\hbar} - \frac{\tau V(\mathbf{R}')}{\hbar} - \frac{\mathrm{mmwD}\,(\mathbf{R},\mathbf{R}')}{\hbar\tau}\right). \tag{8}$$

To get a normalized probability of going from structure $\mathbf{R}$ to structure $\mathbf{R}'$ in the negative imaginary time step, Δt, we can take the ratio of $p(\mathbf{R} \to \mathbf{R}')$ to the probability of staying given by $p(\mathbf{R} \to \mathbf{R})$ $= \mathcal{N}^2\exp(-2\tau V(\mathbf{R})/\hbar)$ (as $\mathrm{mmwD}(\mathbf{R},\mathbf{R}) = 0$). Thus, the normalized probability can be written as

$$\begin{aligned}P(\mathbf{R} \to \mathbf{R}') &= \min\left\{\frac{p(\mathbf{R} \to \mathbf{R}')}{p(\mathbf{R} \to \mathbf{R})}, 1\right\} \\ &= \min\left\{\exp\left(\frac{\tau(V(\mathbf{R}) - V(\mathbf{R}'))}{\hbar}\right.\right. \\ &\quad\left.\left. - \frac{\mathrm{mmwD}\,(\mathbf{R},\mathbf{R}')}{\hbar\tau}\right), 1\right\}.\end{aligned} \tag{9}$$

Here and afterward, we set an upper limit on the probability, as every structure $\mathbf{R}'$ that is more probable than the current structure $\mathbf{R}$ will be accepted, as is done in the Metropolis algorithm.[40] Such a definition of transition probability is one of many that satisfy the detailed balance principle.

To perform the sampling, we need to "mutate" each current structure $\mathbf{R}$ to produce a trial structure $\mathbf{R}'$. We can do that by many different distributions, but the simplest approach is to use the same distribution for kinetic energy defined with the imaginary

time step $\Delta t = -i\tau$. In particular, we can set a new coordinate for a randomly chosen nth atom $(1 \le n \le N)$ as $\mathbf{r}'_n = \mathbf{r}_n + \delta\mathbf{r}_n$, where the displacement $\delta\mathbf{r}_n$ is chosen through the Gaussian distribution,

$$\rho(\delta\mathbf{r}_n) = \left(\frac{2m_n}{\hbar\tau}\right)^{3/2} \exp\left(-\frac{m_n\delta\mathbf{r}_n^2}{\hbar\tau}\right) = \left(2\pi\sigma_n^2\right)^{-3/2} \exp\left(-\frac{\delta\mathbf{r}_n^2}{2\sigma_n^2}\right), \tag{10}$$

where $\sigma_n = \sqrt{\hbar\tau/(2m_n)}$ is the standard deviation for the displacement. The whole algorithm for generating a single trial structure looks as follows. First, a random atom number n is chosen from a uniform distribution. Then, this atom's displacement is generated using the distribution from Eq. (10). As the structure produced in this way will disturb the center of mass position, the structure is recentered, producing the trial structure $\mathbf{R}'$. This procedure is also similar in spirit to the simplified Wigner sampling introduced in Refs. 41 and 42; therefore, as a guess for the optimal effective inverse temperature $\beta = \tau/\hbar$, we use the heuristic criterion for τ from Ref. 42, given as

$$\tau = \frac{1}{2\pi\langle\nu\rangle}, \tag{11}$$

where $\langle\nu\rangle$ is the average of all harmonic frequencies of a given molecule.

The last ingredient for the reaction path search is the directional bias of one structure to another. For this, we use the proximity between structures defined exclusively from a kinetic energy perspective through the probability,

$$\tilde{p}(\mathbf{R} \to \mathbf{R}') = \frac{\left|\langle\mathbf{R}'|\exp\left(-\tau_{\text{inter}}\frac{1}{\hbar}\hat{T}\right)|\mathbf{R}\rangle\right|^2}{\left|\langle\mathbf{R}|\exp\left(-\tau_{\text{inter}}\frac{1}{\hbar}\hat{T}\right)|\mathbf{R}\rangle\right|^2} = \exp\left(-\frac{\text{mmwD}\ (\mathbf{R},\mathbf{R}')}{\hbar\tau_{\text{inter}}}\right), \tag{12}$$

where $\tau_{\text{inter}} = N_{\text{inter}} \times \tau$ is the effective inverse temperature for interconversion between distant structures and $N_{\text{inter}} > 0$ is a parameter controlling the softness of the bias (small $N_{\text{inter}} \le 1$ indicates strong bias, and $N_{\text{inter}} > 1$ indicates weakened bias). The probability from Eq. (12) will be used to differentiate between trial structures going toward the desired reactant/product and away from it from a pure molecular geometry perspective, without taking into account the PES, as the more similar pairs of structures correspond to larger values of $\tilde{p}(\mathbf{R} \to \mathbf{R}')$.

With all this instrumentation, the algorithm looks as follows.

- We choose two initial structures for the reactant and product, $\mathbf{R}_{\text{r}}^{(0)}$ and $\mathbf{R}_{\text{p}}^{(0)}$, respectively, and compute their potential energies $V(\mathbf{R}_{\text{r}}^{(0)})$ and $V(\mathbf{R}_{\text{p}}^{(0)})$. From here on, index "r" will denote the reactant and index "p" will denote the product.
- Then, we iterate between the reactant and product, moving the MC simulations forward for both reactant and product. Essentially, we are simultaneously driving two Metropolis MC[40] trajectories: one for the reactant and one for the product.
  - The corresponding structures at iteration i are $\mathbf{R}_X^{(i)}$ and $\mathbf{R}_Y^{(i)}$ $(X, Y = \text{r}, \text{p})$.
  - Now, we generate the next trial structure $\mathbf{R}'_X$ for the current $X = \text{r}, \text{p}$, while its counterpartner $Y = \text{p}, \text{r}$ is fixed. For this, we produce a preselection of structures using the kinetic energy probability from Eq. (12).
    - Generate a trial structure $\tilde{\mathbf{R}}'_X$ from the distribution given in Eq. (10), as described in the discussion to this equation.
    - Compute the probability of acceptance as defined through Eq. (12) as

$$\begin{aligned} P_{\text{acc}}(\tilde{\mathbf{R}}'_X \to \mathbf{R}'_X) &= \min\left\{\frac{\tilde{p}(\tilde{\mathbf{R}}'_X \to \mathbf{R}_Y^{(i)})}{\tilde{p}(\mathbf{R}_X^{(i)} \to \mathbf{R}_Y^{(i)})}, 1\right\} \\ &= \min\left\{\exp\left(\frac{\text{mmwD}\ (\mathbf{R}_X^{(i)}, \mathbf{R}_Y^{(i)})}{\hbar\tau_{\text{inter}}}\right.\right. \\ &\quad \left.\left. - \frac{\text{mmwD}\ (\tilde{\mathbf{R}}'_X, \mathbf{R}_Y^{(i)})}{\hbar\tau_{\text{inter}}}\right), 1\right\}. \end{aligned} \tag{13}$$

      This probability is biased to be higher for trial structures $\tilde{\mathbf{R}}'_X$ that are more geometrically similar to the current structure $\mathbf{R}_Y^{(i)}$ of Y, than the current $\mathbf{R}_X^{(i)}$ of X.
    - We draw a number $0 \le p_{\text{trial}} < 1$ from a uniform distribution. If $p_{\text{trial}} \le P_{\text{acc}}(\tilde{\mathbf{R}}'_X \to \mathbf{R}'_X)$, we accept the generated structure $\tilde{\mathbf{R}}'_X$ as $\mathbf{R}'_X$. However, if $p_{\text{trial}} > P_{\text{acc}}(\tilde{\mathbf{R}}'_X \to \mathbf{R}'_X)$, we generate a new structure $\tilde{\mathbf{R}}'_X$ and perform the procedure again, until a new structure is generated or an arbitrarily set number of iterations (100 in this work) is reached. This maximal number of iterations is required to avoid endless loops if the parameters of the simulation are improperly chosen.

    We perform this preselection of structures because it is computationally inexpensive, as it does not require the calculation of potential energies, $V(\tilde{\mathbf{R}}'_X)$, but it assures that we force the structures from the reactant side of the reaction and the structures from the product side to get closer to each other as the MC simulation proceeds.
  - For the generated trial structure, we compute the potential energy of the trial structure $V(\mathbf{R}'_X)$ and then the acceptance probability $P(\mathbf{R}_X^{(i)} \to \mathbf{R}'_X)$ using Eq. (9).
  - We draw again a random number p_{trial} and if $p_{\text{trial}} \le P(\mathbf{R}_X^{(i)} \to \mathbf{R}'_X)$, we accept the trial structure $\mathbf{R}'_X$ as the new geometry for X (i.e., $\mathbf{R}_X^{(i+1)} = \mathbf{R}'_X$). If the trial geometry is discarded, i.e., $p_{\text{trial}} > P(\mathbf{R}_X^{(i)} \to \mathbf{R}'_X)$, then the structure of X remains unchanged $(\mathbf{R}_X^{(i+1)} = \mathbf{R}_X^{(i)})$.
- By performing this procedure, we propagate reactant and product trajectories one after another until either a prechosen number of steps is reached or the two structures $\mathbf{R}_{\text{r}}^{(i)}$ and $\mathbf{R}_{\text{p}}^{(i)}$ become very close to each other. As a criterion for this, we consider the distribution for generating trial

structures Eq. (10). With this, if we displace all the atoms simultaneously, the mean mwMSD between initial and displaced structures is $\langle \text{mwMSD} \rangle = 3N\hbar\tau/2$. Therefore, as a criterion for stopping the simulation, we use

$$\frac{2\,\text{mmwD}\,(\mathbf{R}_\text{r}^{(i)}, \mathbf{R}_\text{p}^{(i)})}{3N\hbar\tau} \le s, \tag{14}$$

where s is a threshold value that we choose to equal unity ($s = 1$).

III. NUMERICAL EXAMPLE

A. Two-dimensional model

As a first application example, we considered a two-dimensional system that emulates bath-coupled proton transfer.[43] The PES for our example was defined as

$$V(x,y) = \overbrace{\frac{V_\text{BH}}{x_0^4}(x-x_0)^2(x+x_0)^2}^{V_\text{PT}(x)} + \overbrace{\frac{f}{2}y^2}^{V_\text{bath}(y)} - \overbrace{\alpha f x y}^{W(x,y)}, \tag{15}$$

where x is the proton transfer coordinate; y is the environment coordinate; $V_\text{PT}(x)$ is a double-well potential of the proton transfer motion parameterized through the minimum position $\pm x_0$ and barrier height V_BH; $V_\text{bath}(y)$ is the harmonic potential of the environment defined via spring constant $f = 4\pi^2 m c^2 \tilde{\nu}^2$, with m being the mass of the bath coordinate, $c = 29\,979\,245\,800$ cm/s being the speed of light, and $\tilde{\nu}$ being the vibrational frequency, expressed in wavenumbers; and $W(x,y)$ is the coupling energy, given through dimensionless coupling strength α. As a set of parameters, we took the effective masses along the proton transfer and bath coordinates equal to $m = 1$ a.m.u., $V_\text{BH} = 23.9$ kJ/mol (2000 cm^{-1}), $x_0 = 0.5$ Å, $\tilde{\nu} = 1000$ cm^{-1}, and $\alpha = 0.7$. These parameters led to two equivalent minima at coordinates $(x_\text{min}, y_\text{min}) = (-0.603, -0.422)$ Å and $(x'_\text{min}, y'_\text{min}) = (0.603, 0.422)$ Å, with a barrier of 50.6 kJ/mol (4229 cm^{-1}) separating these potential wells. The harmonic frequencies in these two wells were 908 and 1950 cm^{-1} for bath and proton-transfer normal modes, respectively, which gave an estimated optimal τ of 3.7 fs according to Eq. (11). An illustration of the PES from Eq. (15) is given in Fig. 1.

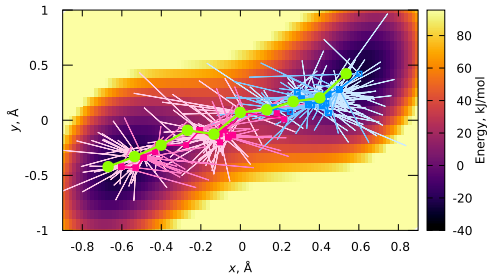

FIG. 1. Two-dimensional potential given in Eq. (15) and a single MC simulation result plotted on top. The pink and blue curves illustrate the following: (1) rejected trials taken in the preselection procedure (the narrowest lines); (2) rejected MC steps (medium-width lines); (3) accepted MC steps (bold lines with square symbols). The green line with circular points indicates the averaged MC path. The parameters for this simulation were $\tau = 3.4$ fs and $N_\text{inter} = 1$. An upper value of 95.7 kJ/mol (8000 cm^{-1}) was set to the energy axis (color scale) to increase the contrast for the low-energy region.

Using this analytical potential, multiple MC reaction path searches between the two minima were run using the algorithm introduced in Sec. II. In this simplified model, the positions were given by two-dimensional vectors $\mathbf{R} = (x, y)$ and thus mmwD Eq. (7), reduced to the mass-weighted squared Euclidean distance between two points, namely,

$$\text{mmwD}(\mathbf{R}, \mathbf{R}') = m\big((x-x')^2 + (y-y')^2\big). \tag{16}$$

The MC trajectories were run with different values of τ ($0.1 \le \tau \le 10$ fs) and N_inter ($0.01 \le N_\text{inter} \le 100$). Ten MC trajectories were produced for each pair of parameters τ and N_inter. In the end, the following parameters were monitored: barrier height, acceptance ratio in the MC procedure (i.e., number of accepted MC trials over total number of steps in MC trajectory), N_bias, defined as the number of steps taken in the structure preselection routine, total trajectory length, and convergence percentage. The maximal number of steps for each single trajectory was set to 10 000 steps, which led to some trajectories never reaching the convergence criterion during the MC simulation. An example of how a single converged MC trajectory looks is given in Fig. 1.

The lengths of MC trajectories are shown in Fig. 2. One can notice that in the range of $1 \le \tau \le 4$ fs and $N_\text{inter} \le 1$, there is a region in which the MC simulations reach convergence faster. In addition, the increase in the N_inter parameter leads to the overall rise of trajectory duration, ultimately leading to convergence of the simulation not being reached in the designated number of steps. For instance, for simulations with $\tau = 3.4$ fs and $N_\text{inter} = 100$, only 80% of the trajectories converged, while for $\tau = 4.5$ fs and $N_\text{inter} = 100$, it was 40%. One can also note that $\tau = 3.7$ fs, determined from the criterion in Eq. (11), is close to the optimal region for the fast MC simulation convergence.

For Metropolis-type MC simulations, an acceptance rate of 23.4% is commonly considered optimal.[44–46] In our simulations, the acceptance rate dropped with the increase in the τ parameter, as shown in Fig. 3. Usage of smaller τ values induces small changes in geometries, which leads to most of the new structures generated being accepted. At the same time, structure generation with large τ values leads to new molecular geometries that are too distorted,

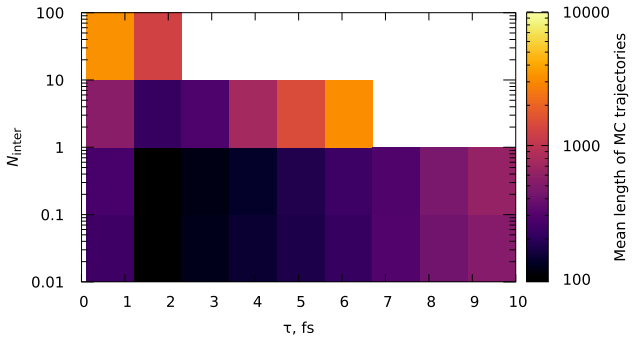

FIG. 2. Mean lengths of the MC trajectories in the two-dimensional model at various parameters τ and N_inter. The empty points indicate that not all trajectories converged.

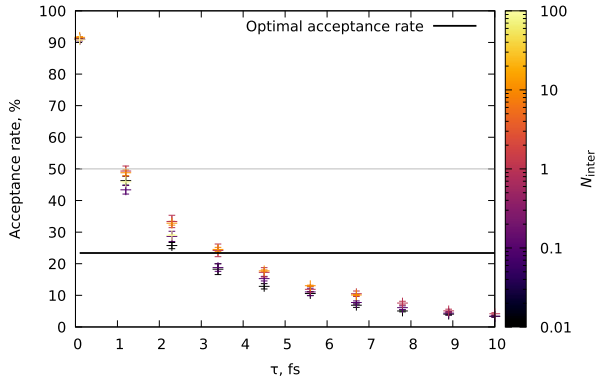

FIG. 3. Acceptance rates for the MC trajectories in the two-dimensional model at various parameters τ and N_{inter}.

and due to the large potential energy increase for the trial structure, most of the generated steps are rejected. The desired acceptance rate of 23.4% is reached for $2 \le \tau \le 5$ fs, which again overlaps with our estimate of $\tau = 3.7$ fs from Eq. (11).

The mean length of the preselection procedure at each step of the MC simulation (N_{bias}) is expected to increase with the decrease in the N_{inter} parameter: the tighter the bias criterion gets, the more selective the acceptance probability will be for structures that lead toward the counterpropagating trajectory. This is exactly what is seen in the simulation results, as shown in Fig. 4. As this stage of the simulation is computationally inexpensive, this increase in the number of intermediate structures by itself is not a problem.

The actual values that are produced by the MCTSS procedure are the reaction barrier heights, which were estimated from using the x-coordinate as a reaction coordinate, and then compressing the trajectories' frames along this axis in between the two equilibrium values of $x = \pm 0.603$ Å into ten equally spaced bins. The barrier for each MC trajectory was computed as an energy difference between the lowest and highest energy bins, and results from different simulations were averaged out to produce the mean barrier and its standard deviation for ten trajectories. The resulting reaction energy profiles obtained from averaging MC results for a given set of τ and

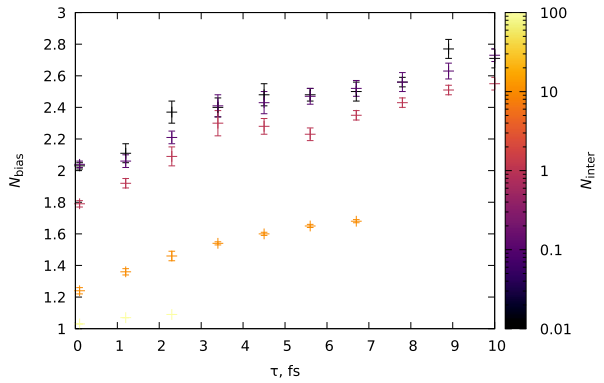

FIG. 4. Number of generated structures at the preselection stage for the MC trajectories in the two-dimensional model at various parameters τ and N_{inter}.

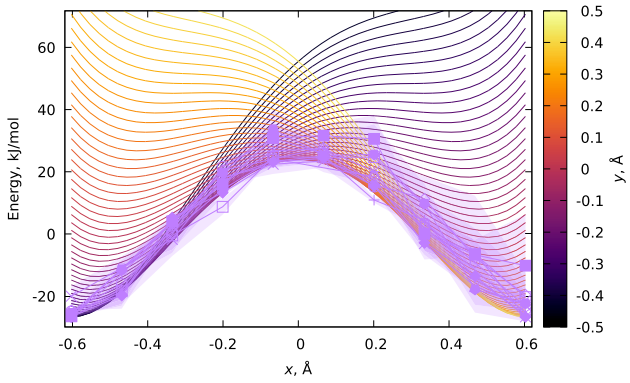

FIG. 5. Projection of the PES Eq. (15) region between the two minima (solid lines with y-coordinate shown via the color scale) and averaged reaction profiles from MC simulations at various parameters τ and N_{inter} (points connected by straight segments). Different point types show different pairs of τ and N_{inter}. The shaded area around the points is the standard error in averaging from different MC trajectories.

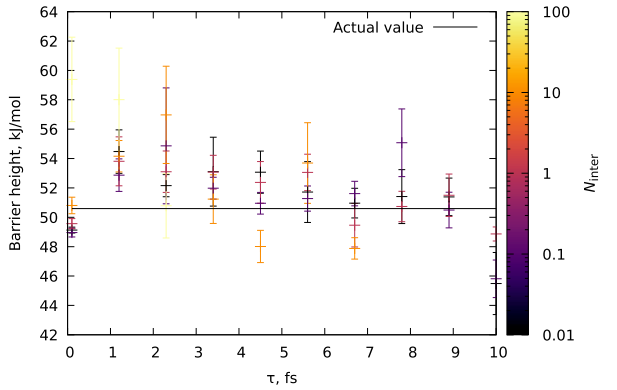

FIG. 6. Average barriers and their standard deviations in multiple MC trajectories in the two-dimensional model at various parameters, τ and N_{inter}.

N_{inter} are shown in Fig. 5, while the barriers from multiple trials with different parameters can be seen in Fig. 6. One can see from the figure that all the converged simulations provide a good agreement between the actual values of the barrier, with the largest relative deviations not exceeding 18%. The variations in the barrier heights, which even lead to lower values than the actual barrier height, appear from sampling of the low and high energy regions on the PES. With these results indicating similar performance of the MC estimates of the barrier heights with different settings and with the presented estimates on the acceptance rate and trajectory lengths, we can conclude that the appropriate choices for the parameters τ and N_{inter} are Eq. (11) for τ and $N_{inter} \le 10$.

B. Molecular example

1. Implementation

The software implementing the algorithm described in Sec. II for arbitrary molecular systems was written in Python using

standard Python library packages (Random and Argparse), as well as the Atomic Simulation Environment (ASE) library[47] in conjunction with ORCA 6[48–50] as the source of the potential energies. The software also uses NumPy[51] for various mathematical operations and SciPy,[52] particularly for the implementation of the Kabsh algorithm. The unit tests for the individual routines were written using the Unittest framework.

2. General considerations

As an exemplary reaction, we chose the S_N2-substitution of bromine in bromomethane (CH_3Br) with a chloride anion, producing a bromide anion and chloromethane (CH_3Cl), namely,

$$Cl^- + CH_3Br \leftrightharpoons ClCH_3 + Br^-. \tag{17}$$

The structures of the reactants and products were optimized at the HF-3c[53] level of theory using ORCA 6 software. As a reference, we performed CI-NEB calculations[29] to find a robust approximation to the optimal reaction pathway. Single-point energy calculations at the DLPNO-CCSD(T)/cc-pVDZ[54,55] level of theory were performed for the pathway found at the HF-3c level of theory.

The MC trajectories were computed at the HF-3c and DLPNO-CCSD(T)/cc-pVDZ levels of theory starting from the HF-3c equilibrium structures of the reactant and the product. We processed the MC trajectories to compute the averaged reaction potential energy profiles. The reaction coordinate was defined as

$$\xi = r(\mathrm{C}\ldots\mathrm{Br}) - r(\mathrm{Cl}\ldots\mathrm{C}), \tag{18}$$

where $r(A\ldots B)$ indicates the distance between atoms A and B. Negative values indicate the reactant in Eq. (17), while positive values of this coordinate correspond to the product.

The whole accessible range of reaction coordinate values for all MC frames was divided into an arbitrary number of subintervals (15, in this work), and the frames of the MC simulation trajectory with reaction coordinate values in these subintervals were averaged to produce the mean potential energy with corresponding standard deviations as well as average structures along this reaction coordinate mapping. The reaction energy profiles from different MC trajectories were then averaged.

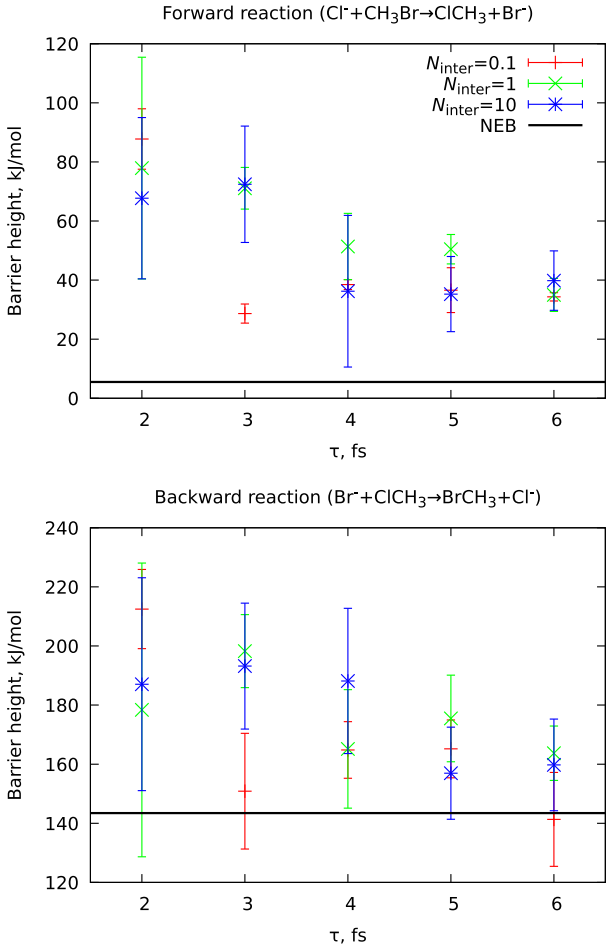

FIG. 7. Barriers for the forward ($Cl^- + CH_3Br \rightarrow ClCH_3 + Br^-$, top) and backward ($Cl^- + CH_3Br \leftarrow ClCH_3 + Br^-$, bottom) S_N2 reaction Eq. (17) computed with MC (points with error bars) at various parameters τ and N_{inter}. The horizontal lines indicate barriers from CI-NEB. All calculations were done at the HF-3c level of theory.

3. Monte Carlo parameter space exploration

Similarly to what was done in Sec. III A, we explored the MC performance with different values for τ and N_{inter}. For this, the following combinations of values were taken: $2 \le \tau \le 6$ fs with 1 fs increment and $N_{\mathrm{inter}} = 0.1, 1, 10$. For computational efficiency, the MC simulations were done at the HF-3c level of theory. The optimal τ, according to Eq. (11), was 3.5 fs for the reactant and 3.4 fs for the product in Eq. (17).

The acceptance rate in all cases was around 50%, which is above the optimal value of 23.4%, but still sufficiently selective to sample the PES. The same trends as observed in Sec. III A persist: the trajectory length decreases and N_{bias} increases with the decrease in N_{inter}, while the acceptance rate increases with the decrease in τ. The barriers for the reaction were found to be somewhat higher than the actual ones, found using CI-NEB (Fig. 7), especially for the lower-barrier forward reaction in Eq. (17). The energy profiles (Fig. 8) of the reaction along the reaction coordinate, obtained from MCTSS, are higher in energy than those from CI-NEB.

However, upon examining the resulting average geometries of the molecular species (Fig. 9), we observe a correspondence between the MCTSS results and the CI-NEB pathway. The energy difference appears from the random displacements in the MC simulations, as the pathway between reactant and product geometries is not energy-optimized. In more detail, we can compare the parameters of the TS from the CI-NEB calculation and the average of the highest-energy frames from the MCTSS simulations, which would correspond to the TS (Table I). The important geometric parameters are the distances between carbon and the halogens ($r(\mathrm{C}\ldots\mathrm{Cl})$ and $r(\mathrm{C}\ldots\mathrm{Br})$) and the mean carbon–hydrogen distance, which we denote as $r_{\mathrm{mean}}(\mathrm{C}\ldots\mathrm{H})$. The last geometric parameter that we monitor is the pyramidization parameter of the CH_3-fragment, which we define, following Ref. 56, as

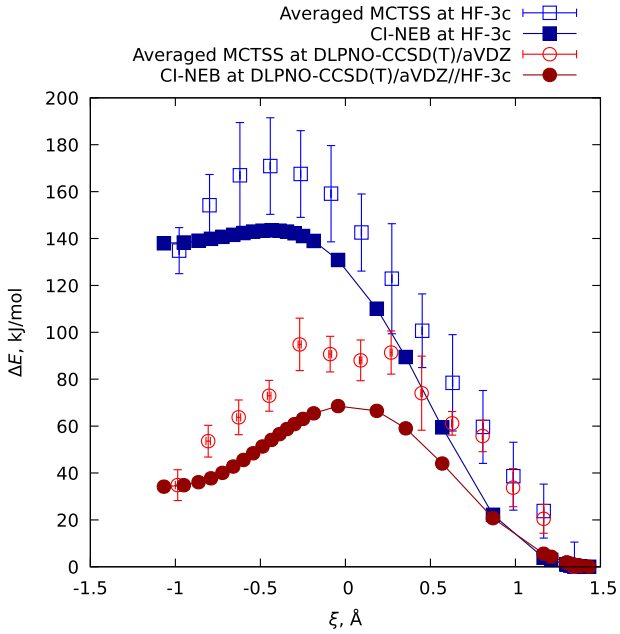

FIG. 8. Potential energy curves for the S_N2 reaction given in Eq. (17). Averaged MCTSS at the HF-3c level of theory is an average curve for 20 calculations, with $\tau = 2, 3, 4, 5, 6$ fs and $N_{inter} = 0.1, 1, 10$. Averaged MCTSS at the DLPNO-CCSD(T)/aug-cc-pVDZ level was computed from five trajectories obtained with $\tau = 4$ fs and $N_{inter} = 0.1, 0.5, 1, 5, 10$. The energy of products in each separate curve is chosen as the reference energy.

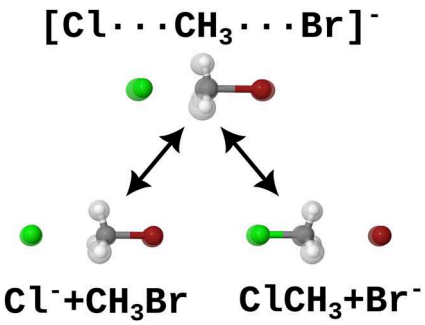

FIG. 9. Geometries of the S_N2 reaction in Eq. (17) at the HF-3c level of theory. The molecular geometries represent the reactant, product, and TS structures from CI-NEB calculations, while the translucent distributions show the distribution of the corresponding structures from the MCTSS calculations, with $\tau = 2, 3, 4, 5, 6$ fs and $N_{inter} = 0.1, 1, 10$.

$$q_{CH_3} = \frac{\mathbf{r}_1 \cdot [\mathbf{r}_2 \times \mathbf{r}_3]}{2S_{HHH}}, \tag{19}$$

where $\mathbf{r}_n$ is the vector from the carbon atom to the nth hydrogen atom, $\mathbf{r}_1 \cdot [\mathbf{r}_2 \times \mathbf{r}_3]$ is the scalar triple product of these three vectors, and S_{HHH} is the area of the triangle formed by the three hydrogens. The parameter q_{CH_3} (given in Å) equals the distance of the carbon to the plane formed by the three hydrogen atoms. The results shown in Table I indicate that the mean distances to the halogens are generally a bit increased compared to the CI-NEB results, which explains the increased energies. However, the CI-NEB and MCTSS results agree within the uncertainties.

TABLE I. Geometric parameters of the TS in the S_N2 reaction given in Eq. (17) from the CI-NEB and MCTSS simulations at the HF-3c level of theory. The MCTSS results are the average of 20 calculations with $\tau = 2, 3, 4, 5, 6$ fs and $N_{inter} = 0.1, 1, 10$.

	Value, Å	
Parameter	CI-NEB	MCTSS
$r(C\ldots Cl)$	2.22	2.36 ± 0.13
$r(C\ldots Br)$	2.66	2.73 ± 0.09
$r_{mean}(C\ldots H)$	1.09	1.09 ± 0.03
q_{CH_3}	−0.17	−0.21 ± 0.10

4. Demonstration of the MCTSS approach for gradient-less methods

To demonstrate the strength of the MCTSS approach, we performed a calculation of the same reaction given in Eq. (17), but with the DLPNO-CCSD(T) method as the source of the potential energy. This quantum-chemical method allows for single-point energy computations of large systems with more than 100 atoms with chemical accuracy.[57] However, no analytical gradients are available for this method and are not expected to appear in the near future due to the inherent complexity of this theoretical approach. For this, we have calculated five MC trajectories at the DLPNO-CCSD(T)/aug-cc-pVDZ level of theory, with $\tau = 4$ fs, chosen from the simulations at the HF-3c level of theory, and $N_{inter} = 0.1, 0.5, 1, 5, 10$. The resulting potential energy curve for the backward-reaction path is given in Fig. 8. The comparison of the MCTSS results was made to the CI-NEB reaction-path geometries obtained at the lower (HF-3c) level of theory with single-point energies computed at the DLPNO-CCSD(T)/aug-cc-pVDZ level of theory, as the CI-NEB procedure requires gradients. As one can see, the averaged MCTSS potential energy curve is still higher in energy than the DLPNO-CCSD(T)/aug-cc-pVDZ//HF-3c profile. However, the direct application of a high-accuracy method for reaction path investigation can be advantageous in cases where lower-cost methods will give divergent results.

IV. DISCUSSION

We have shown the applicability of the proposed MC approach for identifying the reaction pathways. The computational routine is physics-driven and allows for a few system-driven parameters to fully define the simulation procedure. The algorithm and calculations we presented here are not optimal, as our goal was to provide a proof-of-principle for this concept. In the case of halogenide ion exchange in halogenated methane Eq. (17), the obtained reaction barriers are somewhat higher in energy than the analogous values found by the CI-NEB. This is most likely due to the linear approximation between the reactant and the product, which forces the simulation to follow a suboptimal linear path, avoiding the TS, rather than the optimal path directly through the TS.[26,58] Another reason may be the stochastic nature of the MCTSS procedure, which yields suboptimal reaction-path geometries due to residual random atom displacements.

There can be various ways to improve the current MCTSS approach. We can include reusing information about previous configurations or an adaptive variation of the bias parameter N_{inter} during the course of the MC simulation. Due to the intrinsic similarity of our approach to the instanton methods for simulating nuclear dynamics,[59] some ideas can also be drawn from this area of research. Further improvements can be obtained by applying a chain-of-states treatment of trajectories: instead of having only two co-propagating structures, one can use multiple pairwise-connected structures, which will provide a higher flexibility of the molecular fragments, especially in the case of highly non-linear reaction paths, such as concerted internal rotation.

Moreover, the MC search of pathways could be useful, e.g., when the initial and final states lie on different potential energy surfaces. For instance, this could be a possible strategy to sample the Marcus rearrangement coordinates upon electron transfer processes[60] or to search for conical intersections between different electronic states, similar to how that was done in Ref. 37.

Another way to adapt this algorithm may be by fixing the structure of the initial/final state, which could be useful for sampling structures to compute, e.g., ultraviolet–visible (UV/vis) absorption and emission spectra.[61] For absorption spectra, the ground state equilibrium geometry should be fixed, whereas for emission spectra, it should be the equilibrium geometry in the excited electronic state. The MC procedure can provide an ensemble of geometries, for which individual electronic spectra can be computed. Such a procedure can be used as an intermediate cost way to include a crude vibrational structure in the UV/vis spectra calculations, which can be advantageous for large molecular systems, for which calculations of Franck–Condon factors and resulting vibronic spectra might be computationally challenging.[62–64]

V. CONCLUSIONS

In this work, we presented an algorithm for searching reaction pathways in molecular systems using a Monte Carlo approach. The method is based on quantum Monte Carlo ideas, namely, on the real-space diffusion Monte Carlo. It requires two structures, initial and final structure guesses, and then two simultaneous Monte Carlo trajectories are driven: one from the initial to the final state and one in the opposite direction. The Monte Carlo steps of both trajectories are biased by a cost-efficient preselection procedure, forcing the two trajectories' frames to get increasingly close as the calculation proceeds. This algorithm was demonstrated numerically using two examples: a two-dimensional model emulating a proton transfer with a one-dimensional bath and an S_N2-substitution of the halogen in halogenated methane.

While the current work provides only a proof-of-principle implementation, the presented algorithm is already advantageous in comparison with the established transition state search methods because of its applicability in conjunction with quantum chemistry methods that do not have analytical gradients implemented, as it relies only on single-point energy calculations. In addition, our algorithm's extensions might be useful for photochemistry, electrochemistry, and spectroscopy calculations.

SUPPLEMENTARY MATERIAL

The source code used in this work and the numerical results are available in the supplementary material as a ZIP archive.

ACKNOWLEDGMENTS

We acknowledge support from DESY (Hamburg, Germany), a member of the Helmholtz Association (HGF). R.S. further acknowledges support from the Cluster of Excellence "CUI: Advanced Imaging of Matter" of the Deutsche Forschungsgemeinschaft (DFG)-EXC 2056-Project ID No. 390715994. Calculations were enabled through the Maxwell computational resources operated at Deutsches Elektronen-Synchrotron DESY, Hamburg, Germany.

AUTHOR DECLARATIONS

Conflict of Interest

The authors have no conflicts to disclose.

Author Contributions

Denis S. Tikhonov: Conceptualization (equal); Formal analysis (equal); Investigation (equal); Methodology (equal); Software (equal); Writing – original draft (equal). **Robin Santra**: Methodology (equal); Project administration (equal); Resources (equal); Supervision (equal); Writing – review & editing (equal).

DATA AVAILABILITY

All the data required to reproduce the results of this paper are available in supplementary material.

REFERENCES

[1] K. J. Laidler and M. C. King, "Development of transition-state theory," J. Phys. Chem. **87**(15), 2657–2664 (1983).
[2] D. G. Truhlar, B. C. Garrett, and S. J. Klippenstein, "Current status of transition-state theory," J. Phys. Chem. **100**(31), 12771–12800 (1996).
[3] O. Eisenstein and S. Shaik, "Computational catalysis: A land of opportunities," Top. Catal. **65**, 1–5 (2022).
[4] B. W. J. Chen, L. Xu, and M. Mavrikakis, "Computational methods in heterogeneous catalysis," Chem. Rev. **121**(2), 1007–1048 (2021).
[5] J. Sauer, "The future of computational catalysis," J. Catal. **433**, 115482 (2024).
[6] I. Funes-Ardoiz and F. Schoenebeck, "Established and emerging computational tools to study homogeneous catalysis—From quantum mechanics to machine learning," Chem **6**(8), 1904–1913 (2020).
[7] V. L. Schramm, "Enzymatic transition states and drug design," Chem. Rev. **118**(22), 11194–11258 (2018).
[8] H. B. Schlegel, "Optimization of equilibrium geometries and transition structures," J. Comput. Chem. **3**(2), 214–218 (1982).
[9] H. P. Hratchian and X. Li, "Thirty years of geometry optimization in quantum chemistry and beyond: A tribute to Berny Schlegel," J. Chem. Theory Comput. **8**(12), 4853–4855 (2012).
[10] C. Peng and H. Bernhard Schlegel, "Combining synchronous transit and quasi-Newton methods to find transition states," Israel J. Chem. **33**(4), 449–454 (1993).
[11] C. J. Cerjan and W. H. Miller, "On finding transition states," J. Chem. Phys. **75**(6), 2800–2806 (1981).
[12] A. Banerjee, N. Adams, J. Simons, and R. Shepard, "Search for stationary points on surfaces," J. Chem. Phys. **89**(1), 52–57 (1985).
[13] J. Hénin, T. Lelièvre, M. R. Shirts, O. Valsson, and L. Delemotte, "Enhanced sampling methods for molecular dynamics simulations [article v1.0]," Living J. Comput. Mol. Sci. **4**(1), 1583 (2022).
[14] A. Laio and M. Parrinello, "Escaping free-energy minima," Proc. Natl. Acad. Sci. U. S. A. **99**(20), 12562–12566 (2002).
[15] J. Comer, J. C. Gumbart, J. Hénin, T. Lelièvre, A. Pohorille, and C. Chipot, "The adaptive biasing force method: Everything you always wanted to know but were afraid to ask," J. Chem. Phys. B **119**(3), 1129–1151 (2015).

[16]A. M. A. West, R. Elber, and D. Shalloway, "Extending molecular dynamics time scales with milestoning: Example of complex kinetics in a solvated peptide," J. Chem. Phys. **126**(14), 145104 (2007).
[17]P. Májek and R. Elber, "Milestoning without a reaction coordinate," J. Chem. Theory Comput. **6**(6), 1805–1817 (2010).
[18]E. Martínez-Núñez, "An automated method to find transition states using chemical dynamics simulations," J. Comput. Chem. **36**(4), 222–234 (2015).
[19]E. Martínez-Núñez, "An automated transition state search using classical trajectories initialized at multiple minima," Phys. Chem. Chem. Phys. **17**, 14912–14921 (2015).
[20]D. J. Wales and J. P. K. Doye, "Global optimization by basin-hopping and the lowest energy structures of Lennard-Jones clusters containing up to 110 atoms," J. Chem. Phys. A **101**(28), 5111–5116 (1997).
[21]Z. Li and H. A. Scheraga, "Monte Carlo-minimization approach to the multiple-minima problem in protein folding," Proc. Natl. Acad. Sci. U. S. A. **84**(19), 6611–6615 (1987).
[22]D. J. Wales and H. A. Scheraga, "Global optimization of clusters, crystals, and biomolecules," Science **285**(5432), 1368–1372 (1999).
[23]X.-X. Lin, Y.-R. Liu, T. Huang, J. Chen, S. Jiang, and W. Huang, "A flexible transition state searching method for atmospheric reaction systems," Chem. Phys. **450–451**, 21–31 (2015).
[24]P. Y. Ayala and H. B. Schlegel, "A combined method for determining reaction paths, minima, and transition state geometries," J. Chem. Phys. **107**(2), 375–384 (1997).
[25]G. Mills, H. Jónsson, and G. K. Schenter, "Reversible work transition state theory: Application to dissociative adsorption of hydrogen," Surf. Sci. **324**(2–3), 305–337 (1995).
[26]H. Jónsson, G. Mills, and K. W. Jacobsen, "Nudged elastic band method for finding minimum energy paths of transitions," in *Classical and Quantum Dynamics in Condensed Phase Simulations* (World Scientific, 1998), pp. 385-404.
[27]S. A. Trygubenko and D. J. Wales, "A doubly nudged elastic band method for finding transition states," J. Chem. Phys. **120**(5), 2082–2094 (2004).
[28]G. Henkelman, B. P. Uberuaga, and H. Jónsson, "A climbing image nudged elastic band method for finding saddle points and minimum energy paths," J. Chem. Phys. **113**(22), 9901–9904 (2000).
[29]V. Ásgeirsson, B. O. Birgisson, R. Björnsson, U. Becker, F. Neese, C. Riplinger, and H. Jónsson, "Nudged elastic band method for molecular reactions using energy-weighted springs combined with eigenvector following," J. Chem. Theory Comput. **17**, 4929–4945 (2021).
[30]E. Weinan, W. Ren, and E. Vanden-Eijnden, "String method for the study of rare events," Phys. Rev. B **66**, 052301 (2002).
[31]B. Peters, A. Heyden, A. T. Bell, and A. Chakraborty, "A growing string method for determining transition states: Comparison to the nudged elastic band and string methods," J. Chem. Phys. **120**(17), 7877–7886 (2004).
[32]P. M. Zimmerman, "Single-ended transition state finding with the growing string method," J. Comput. Chem. **36**(9), 601–611 (2015).
[33]S. J. Avis, J. R. Panter, and H. Kusumaatmaja, "A robust and memory-efficient transition state search method for complex energy landscapes," J. Chem. Phys. **157**(12), 124107 (2022).
[34]D. Hait, J. D. Estrada Pabón, M. Stöhr, and T. J. Martínez, "Locating *ab initio* transition states via geodesic construction on machine-learned potential energy surfaces," J. Chem. Theory Comput. **21**(22), 11632–11644 (2025).
[35]J. Toulouse, R. Assaraf, and C. J. Umrigar, "Chapter fifteen - Introduction to the variational and diffusion Monte Carlo methods," in *Electron Correlation in Molecules—Ab Initio Beyond Gaussian Quantum Chemistry*, edited by P. E. Hoggan and T. Ozdogan (Academic Press, 2016), pp. 285–314.
[36]B. M. Austin, D. Y. Zubarev, and W. A. Lester, Jr., "Quantum Monte Carlo and related approaches," Chem. Rev. **112**(1), 263–288 (2012).
[37]V. Scutelnic, D. S. Tikhonov, S. M. Poullain, E. A. Haugen, A. Attar, L. Barreau, K. Chang, A. P. Fidler, J. D. Gaynor, Y.-C. Lin, J. Yang, E. G. Champenois, X. Wang, X. Shen, L. Duan, F. Ji, S. Weathersby, Y. V. Vishnevskiy, M. Schnell, T. J. A. Wolf, M.-F. Lin, and S. R. Leone, "Capturing ring opening in photoexcited enolic acetylacetone upon hydrogen bond dissociation by ultrafast electron diffraction," J. Phys. Chem. Lett. **16**, 5068–5075 (2025).
[38]R. P. Feynman and A. R. Hibbs, *Quantum Mechanics and Path Integrals*, *International Series in Pure and Applied Physics* (McGraw-Hill, New York, NY, 1965), https://cds.cern.ch/record/100771.
[39]W. Kabsch, "A solution for the best rotation to relate two sets of vectors," Acta Crystallogr., Sect. A **32**(5), 922–923 (1976).
[40]N. Metropolis, A. W. Rosenbluth, M. N. Rosenbluth, A. H. Teller, and E. Teller, "Equation of state calculations by fast computing machines," J. Chem. Phys. **21**(6), 1087–1092 (1953).
[41]D. S. Tikhonov and Y. V. Vishnevskiy, "Describing nuclear quantum effects in vibrational properties using molecular dynamics with Wigner sampling," Phys. Chem. Chem. Phys. **25**, 18406–18423 (2023).
[42]D. S. Tikhonov, "PyRAMD scheme: A protocol for computing the infrared spectra of polyatomic molecules using ab initio molecular dynamics," Spectrosc. J. **2**(3), 171–187 (2024).
[43]W. Li, D. S. Tikhonov, and M. Schnell, "Double proton transfer across a table: The formic acid dimer–fluorobenzene complex," Angew. Chem., Int. Ed. **60**(49), 25674–25679 (2021).
[44]G. O. Roberts, A. Gelman, and W. R. Gilks, "Weak convergence and optimal scaling of random walk Metropolis algorithms," Ann. Appl. Probab. **7**(1), 110–120 (1997).
[45]J. Yang, G. O. Roberts, and J. S. Rosenthal, "Optimal scaling of random-walk Metropolis algorithms on general target distributions," Stochastic Processes Appl. **130**(10), 6094–6132 (2020).
[46]A. Li, L. Wang, T. Dou, and J. S. Rosenthal, "Exploring the generalizability of the optimal 0.234 acceptance rate in random-walk Metropolis and parallel tempering algorithms," arXiv:2408.06894 (2024).
[47]A. Hjorth Larsen, J. Jørgen Mortensen, J. Blomqvist, I. E. Castelli, R. Christensen, M. Dułak, J. Friis, M. N. Groves, B. Hammer, C. Hargus, E. D. Hermes, P. C. Jennings, P. Bjerre Jensen, J. Kermode, J. R. Kitchin, E. Leonhard Kolsbjerg, J. Kubal, K. Kaasbjerg, S. Lysgaard, J. B. Maronsson, T. Maxson, T. Olsen, L. Pastewka, A. Peterson, C. Rostgaard, J. Schiøtz, O. Schütt, M. Strange, K. S. Thygesen, T. Vegge, L. Vilhelmsen, M. Walter, Z. Zeng, and K. W. Jacobsen, "The atomic simulation environment—A Python library for working with atoms," J. Phys.: Condens. Matter **29**(27), 273002 (2017).
[48]F. Neese, "The ORCA program system," Wiley Interdiscip. Rev.: Comput. Mol. Sci. **2**(1), 73–78 (2012).
[49]F. Neese, F. Wennmohs, U. Becker, and C. Riplinger, "The ORCA quantum chemistry program package," J. Chem. Phys. **152**(22), 224108 (2020).
[50]F. Neese, "Software update: The ORCA program system—Version 5.0," Wiley Interdiscip. Rev.: Comput. Mol. Sci. **12**(5), e1606 (2022).
[51]C. R. Harris, K. J. Millman, S. J. van der Walt, R. Gommers, P. Virtanen, D. Cournapeau, E. Wieser, J. Taylor, S. Berg, N. J. Smith, R. Kern, M. Picus, S. Hoyer, M. H. van Kerkwijk, M. Brett, A. Haldane, J. F. del Río, M. Wiebe, P. Peterson, P. Gérard-Marchant, K. Sheppard, T. Reddy, W. Weckesser, H. Abbasi, C. Gohlke, and T. E. Oliphant, "Array programming with NumPy," Nature **585**(7825), 357–362 (2020).
[52]P. Virtanen, R. Gommers, T. E. Oliphant, M. Haberland, T. Reddy, D. Cournapeau, E. Burovski, P. Peterson, W. Weckesser, J. Bright, S. J. van der Walt, M. Brett, J. Wilson, K. J. Millman, N. Mayorov, A. R. J. Nelson, E. Jones, R. Kern, E. Larson, C. J. Carey, İ. Polat, Y. Feng, E. W. Moore, J. VanderPlas, D. Laxalde, J. Perktold, R. Cimrman, I. Henriksen, E. A. Quintero, C. R. Harris, A. M. Archibald, A. H. Ribeiro, F. Pedregosa, P. van Mulbregt, A. Vijaykumar *et al.*, "SciPy 1.0: Fundamental algorithms for scientific computing in python," Nat. Methods **17**, 261–272 (2020).
[53]R. Sure and S. Grimme, "Corrected small basis set Hartree–Fock method for large systems," J. Comput. Chem. **34**(19), 1672–1685 (2013).
[54]Y. Guo, C. Riplinger, U. Becker, D. G. Liakos, Y. Minenkov, L. Cavallo, and F. Neese, "Communication: An improved linear scaling perturbative triples correction for the domain based local pair-natural orbital based singles and doubles coupled cluster method [DLPNO-CCSD(T)]," J. Chem. Phys. **148**(1), 011101 (2018).
[55]T. H. Dunning, "Gaussian basis sets for use in correlated molecular calculations. I. The atoms boron through neon and hydrogen," J. Chem. Phys. **90**(2), 1007–1023 (1989).
[56]D. S. Tikhonov, "A simplistic computational procedure for tunneling splittings caused by proton transfer," Struct. Chem. **33**(2), 351–362 (2022).

[57]Y. Minenkov, E. Chermak, and L. Cavallo, "Accuracy of DLPNO–CCSD(T) method for noncovalent bond dissociation enthalpies from coinage metal cation complexes," J. Chem. Theory Comput. **11**(10), 4664–4676 (2015).
[58]G. Henkelman, G. Jóhannesson, and H. Jónsson, *Methods for Finding Saddle Points and Minimum Energy Paths* (Springer, Netherlands, Dordrecht, 2002), pp. 269–302, ISBN: 978-0-306-46949-7.
[59]J. O. Richardson, "Ring-polymer instanton theory," Int. Rev. Phys. Chem. **37**(2), 171–216 (2018).
[60]R. A. Marcus, "Electron transfer reactions in chemistry: Theory and experiment (nobel lecture)," Angew. Chem., Int. Ed. Engl. **32**(8), 1111–1121 (1993).
[61]S. Del Galdo, B. Chandramouli, G. Mancini, and V. Barone, "Assessment of multi-scale approaches for computing UV–Vis spectra in condensed phases: Toward an effective yet reliable integration of variational and perturbative QM/MM approaches," J. Chem. Theory Comput. **15**(5), 3170–3184 (2019).
[62]S. Gozem and A. I. Krylov, "The *ezSpectra* suite: An easy-to-use toolkit for spectroscopy modeling," WIREs Comput. Mol. Sci. **12**(2), e1546 (2022).
[63]A. Y. Freidzon, R. R. Valiev, and A. A. Berezhnoy, "*Ab initio* simulation of pyrene spectra in water matrices," RSC Adv. **4**, 42054–42065 (2014).
[64]P. S. Rukin, A. Y. Freidzon, A. V. Scherbinin, V. A. Sazhnikov, A. A. Bagaturyants, and M. V. Alfimov, "Vibronic bandshape of the absorption spectra of dibenzoylmethanatoboron difluoride derivatives: Analysis based on *ab initio* calculations," Phys. Chem. Chem. Phys. **17**, 16997–17006 (2015).